ELSEVIER

Materials Science and Engineering A329–331 (2002) 686–695

MATERIALS SCIENCE & ENGINEERING A

www.elsevier.com/locate/msea

Microstructure of Al_3Sc with ternary transition-metal additions

Y. Harada *, D.C. Dunand

Department of Materials Science and Engineering, Northwestern University, 2225 N. Campus Drive, Evanston, IL 60208-3108, USA

Abstract

The microstructure of binary Al_3Sc and ternary $Al_3(Sc_{1-y}X_y)$, where X is one of the transition metals from Group IIIA (Y), IVA (Ti, Zr or Hf) or VA (V, Nb or Ta), was investigated as a function of alloying element concentration for $0.1 \leq y \leq 0.75$. Alloys with Group IIIA and IVA additions exhibited a single $L1_2$ solid-solution phase with some Kirkendall porosity. At the highest concentration studied, a second phase precipitated with the $D0_{19}$ (Y), $D0_{22}$ (Ti) or $D0_{23}$ (Zr and Hf) structure. Conversely, alloys with Group VA additions exhibited both the $L1_2$ trialuminide phase and a dendritic trialuminide second phase with $D0_{22}$ structure for all concentrations studied. The solubility limit in the ternary $L1_2$-type $Al_3(Sc_{1-y}X_y)$ phase was high for Group IIIA and IVA metals (almost 12.5 at.% or $y = 0.5$), and much lower for Group VA metals (from about 1.8 at.% or $y = 0.07$ for Ta to about 2.7 at.% or $y = 0.11$ for V). Similarly, the solubility limit of Sc in the non-$L1_2$ phases decreases from the Group IIIA trialuminide to the Group VA trialuminides. The lattice parameter of the $L1_2$ solid-solution decreased linearly with increasing concentration of Group IVA and VA metals, but increased linearly with concentration of Y (Group IIIA). This linear concentration dependence of the lattice parameter is found to correlate with the atomic size mismatch between Sc and the transition metal. The microhardness of the $L1_2$ solid-solution increased linearly with increasing concentration of ternary elements. The concentration dependence of hardness is strongest for Group VA metals and weakest for Group IVA metals, for which a correlation is found with the concentration dependence of lattice parameter. © 2002 Elsevier Science B.V. All rights reserved.

Keywords: $L1_2$-trialuminides; Microstructure; Lattice parameter; Microhardness

1. Introduction

Among intermetallic compounds, the transition-metal trialuminides are of interest because of their low density, high melting point, good oxidation resistance and potentially useful high-temperature strength for aerospace and automotive applications. These trialuminides are, however, brittle and exhibit non-cubic structures (e.g., $D0_{22}$ for Al_3Ti, Al_3V, Al_3Nb and Al_3Ta, $D0_{19}$ for Al_3Y and Al_3La, and $D0_{23}$ for Al_3Zr and Al_3Hf [1]), except for Al_3Sc which has the cubic $L1_2$ structure. Intermetallics with the latter structure are expected to show enhanced ductility, because of the high crystallographic symmetry and thus, the high number of possible slip systems. There has thus been considerable interest in alloyed trialuminides for which the $L1_2$ structure can be stabilized, e.g. $(Al, X)_3Ti$, where Al is partially substituted for by X as V, Cr, Mn, Fe, Co, Ni or Zn [2–4]. Indeed, limited bending ductility has been reported for $(Al_{0.68}Cr_{0.32})_3Ti$ after hot-extrusion [5] or hot-isostatic pressing [6]. Besides being the only binary transition-metal trialuminide with a stable $L1_2$ structure, Al_3Sc has also the lowest density of all transition-metal trialuminides (3.03 Mg m^{-3}[7]), making it attractive for structural applications. Despite its $L1_2$ structure, polycrystalline Al_3Sc is brittle at room temperature [8], with fracture occurring in a transgranular manner by cleavage primarily on {011} planes. Partial substitution of Sc by other elements may increase the ductility of Al_3Sc (as observed in other intermetallics) and also decrease the cost of the alloy. However, very little is known about the alloying behavior of Al_3Sc, with the exception of a recent study showing that creep properties of Al_3Sc were significantly improved by additions of Y, Ti, Zr and Hf in solid-solution [9]. The alloying behavior of Al_3Sc is also important for the rational design of Sc-containing aluminum alloys, in which small volume fractions of coherent Al_3Sc particles are precipitated [10]. In

* Corresponding author. Present address: Institute of Mechanical Systems Engineering, National Institute of Advanced Industrial Science and Technology, Namiki 1-2, Tsukuba, Ibaraki 305-8564, Japan. Tel.: +81-298-61-7169; fax: +81-298-61-7167.

E-mail address: harada.y@aist.go.jp (Y. Harada).

0921-5093/02/$ - see front matter
PII: S0921-5093(01)01608-2

multicomponent alloys, these Al_3Sc precipitates often contain other alloying elements in solid-solution [11], which can improve the strength and coarsening resistance of the precipitates. In the present study, the microstructure of binary and ternary Al_3Sc, where scandium is replaced substitutionally by Group IIIA, IVA or VA transition-metals, is investigated as a function of the alloying element concentration.

2. Experimental procedures

Button ingots of binary Al_3Sc and ternary $Al_3(Sc, X)$, where X was chosen from the transition-metals of Groups IIIA (Y), IVA (Ti, Zr or Hf) or VA (V, Nb or Ta), were prepared by non-consumable electrode arc-melting on a water-cooled copper hearth under a purified argon atmosphere. A total of 21 different ternary compositions were prepared with stoichiometry $Al_3(Sc_{1-y}X_y)$ where $y = 0.10$, 0.25, 0.50 for X = V, Y, Nb, Hf and Ta, and $y = 0.25$, 0.50, 0.75 for X = Ti and Zr. Initial charges consisted of about 3 g of high-purity metals; 99.94 wt.% pure scandium from Stanford Materials (San Mateo, CA) and 99.99 wt.% pure aluminum from Johnson Matthey (Ward Hill, MA), with appropriate ternary additions of 99.999 wt.% pure titanium, 99.7 wt.% pure vanadium, 99.9 wt.% pure yttrium, 99.94 wt.% pure zirconium, 99.97 wt.% pure niobium, 99.97 wt.% pure hafnium or 99.95 wt.% pure tantalum (all from Johnson Matthey). First, some sacrificial titanium was melted in the arc furnace to getter residual reactive gases from the chamber. Next, melting of the charge was performed four or more times, flipping the charge after each solidification to ensure complete mixing of the metals. The resulting ingots exhibited a weight loss of less than 0.5% with respect to the initial charge. Finally, the ingots were homogenized for 2 h in vacuum (10^{-4} Pa) at 1473 K.

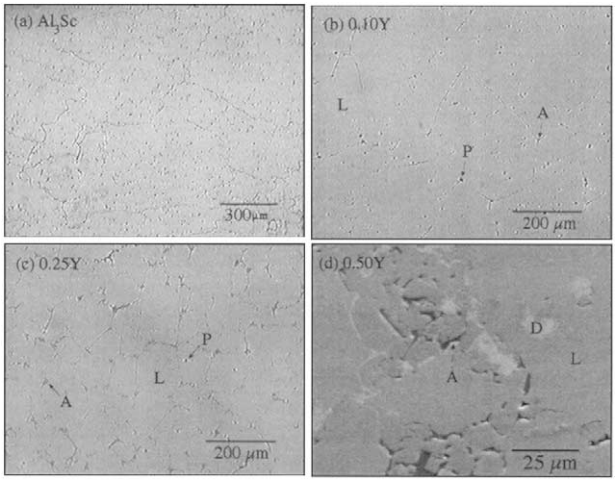

Fig. 1. Typical microstructures of (a) homogenized, etched binary Al_3Sc and (b)–(d) homogenized $Al_3(Sc_{1-y}X_y)$ with X as yttrium for $y = 0.10$, 0.25 and 0.50. (A: Al phase, L: $L1_2$ phase, D: $D0_{19}$ phase and P: porosity).

Metallographic preparation consisted of mounting and polishing with SiC paper and 0.05 μm Al_2O_3 as well as, in some instances, etching with a 10 vol.% HF aqueous solution. Energy dispersive X-ray spectroscopy (EDS), scanning electron microscopy (SEM), and wet chemical analysis (Luvak, Inc., Boylston, MA) were also performed to obtain the compositions of the bulk samples and individual phases.

Portions of the homogenized ingots were pulverized and the resulting powders, sieved to less than 250 mesh size (75 μm), were analyzed by X-ray diffraction (XRD) using CuK_α radiation. Lattice parameters were calculated by the least-squares method using the JADE program (Materials Data Inc., Livermore, CA).

Homogenized specimens were cut along a plane perpendicular to the surface of the ingot that had been in contact with the water-cooled copper hearth. After polishing, the Vickers micro-hardness of the $L1_2$ matrix phase was measured using a 200 g load and an indentation time of 10 s, with the average and standard deviation of 10 measurements reported.

3. Results and discussion

3.1. Microstructure

The binary Al_3Sc was found by X-ray diffraction to have the $L1_2$ structure with a lattice parameter $a = 4.103(1)$ Å, in good agreement with earlier results [7]. The bulk composition was 74.8 at.% Al–25.2 at.% Sc as measured by wet chemical analysis and this value was used to calibrate the EDS detector. The microstructures of homogenized Al_3Sc and $Al_3(Sc_{1-y}X_y)$ (Group IIIA) specimens are shown in Fig. 1. These micrographs indicate that the materials exhibit somewhat large columnar grains with their long axis (average size of 600 μm) perpendicular to the water-cooled copper hearth. Voids (typical size of 5 μm) and precipitates (typical size of 5 μm) were observed in the grain interior. Incongruent, non-equilibrium solidification of a melt with Al_3Sc composition leads to a microstructure consisting of Al_2Sc and Al–Al_3Sc eutectic [12]. Homogenization of the alloy to the equilibrium single-phase Al_3Sc microstructure is achieved by reaction of Al with Al_2Sc, which produces Kirkendall porosity because of the high diffusivity of Al. The second phases are attributed to the facts that Al_3Sc is a line compound and that the initial composition was slightly scandium-rich. Although, some oxygen contamination was expected from the presence of oxides on the pure metals, the measured oxygen content of Al_3Sc was fairly low (0.0035 wt.%).

The as-cast ternary alloys exhibited a segregated microstructure consisting of a single majority phase with a low volume fraction of a grain-boundary phase as well as a second phase within grains in some case. These phases are expected to be Al_3(Sc, X), Al and Al_3(X, Sc), respectively, as a result of segregation from the rather high solidification rate of the alloy. The Al-phase disappeared to a large extent after the homogenization treatment but, as expected, significant Kirkendall porosity developed.

Microstructures of homogenized $Al_3(Sc_{1-y}X_y)$ alloys with X as yttrium for $0.1 \leq y \leq 0.50$ are shown in Fig. 1(b)–(d). These ternary alloys exhibit a segregated microstructure consisting of a single majority $L1_2$ Al_3(Sc, Y) phase with a low volume fraction of Al phase at grain boundaries. Kirkendall porosity (~ 50 μm) is developed with increasing Y additions (~ 50 μm) at the grain boundaries. For equal amounts of yttrium and scandium ($y = 0.50$), a dendritic second phase is observed, which is confirmed by XRD to be the $D0_{19}$ phase Al_3Y with some Sc replacing Y (Table 1).

Fig. 2 shows microstructures of ternary $Al_3(Sc_{1-y}X_y)$ for $0.1 \leq y \leq 0.75$, with X being titanium, zirconium or hafnium (Group IVA). These alloys exhibit microstructures consisting of a single majority phase with a low volume fraction of the Al phase at grain boundaries. The Kirkendall porosity increases with increasing concentration of ternary alloying elements. For $y = 0.5$ these alloys contain a low volume fraction of the $D0_{22}$ phase (for Ti) or $D0_{23}$ phase (for Zr or Hf). In the case of Ti for $y = 0.75$, the material consists of the $D0_{22}$ phase with composition, $Al_3(Ti_{0.81}Sc_{0.19})$, with no $L1_2$ phase present (Table 1). In the case of Zr for $y = 0.75$, dendritic $L1_2$ and $D0_{23}$ phases coexist. These phase were confirmed by EDS and XRD analyses to be $Al_3(Sc_{0.5}Zr_{0.5})$ with the $L1_2$ structure and $Al_3(Zr_{0.87}Sc_{0.13})$ with the $D0_{23}$ structure (Table 1).

Figure 3 displays microstructures of ternary $Al_3(Sc_{1-y}X_y)$ for $0.1 \leq y \leq 0.50$ with X being vanadium, niobium or tantalum (Group VA). All alloys exhibit Kirkendall porosity (~ 80 μm) and they contain a second phase with a dendritic structure whose fraction increases with increasing content of ternary additions. These second phases were confirmed by EDS to be $Al_3(V_{0.97}Sc_{0.03})$, $Al_3(Nb_{0.95}Sc_{0.05})$ or $Al_3(Ta_{0.91}Sc_{0.09})$, independent of the overall composition (Table 1).

Fig. 4 shows typical X-ray diffraction patterns of $Al_3(Sc_{1-y}X_y)$ with X as yttrium (Group IIIA), titanium (Group IVA) or vanadium (Group VA). As described below, the X-ray diffraction patterns evolve with increasing ternary alloying element concentrations, in agreement with the metallographic and EDS observations reported above.

For Ti additions (Fig. 4(a)), the Bragg peaks of the $L1_2$ phase are shifted to higher angles with increasing Ti content. For $y = 0.25$, only the $L1_2$ phase with Al_3Sc composition is present, while for $y = 0.50$ and 0.75, the $D0_{22}$ phase with Al_3Ti composition is formed. It is clear that this alloy transforms from the $L1_2$ to the $D0_{22}$ structure with increasing Ti content. This result is in good agreement with earlier results; Kita et al. [13] reported that Al_3Ti with the $D0_{22}$ the structure, where Ti is replaced by Sc, formed the $L1_2$ structure for the composition $Al_3(Ti_{0.5}Sc_{0.5})$. In the cases of Zr or Hf, we find similarly that our alloys transform from the $L1_2$ structure with Al_3Sc composition to the $D0_{23}$ structure with Al_3Zr or Al_3Hf compositions.

For V additions (Fig. 4(b)), the $Al_3(V_{0.97}Sc_{0.03})$ phase with $D0_{22}$ structure exists in addition to the $L1_2$ phase. The XRD patterns for Al_3(Sc, V) alloys are similar to those of Al_3(Sc, Nb) and Al_3(Sc, Ta), for which the $D0_{22}$ phase is also observed together with the $L1_2$ phase, thus confirming that $Al_3(Nb_{0.95}Sc_{0.05})$ and $Al_3(Ta_{0.91}Sc_{0.09})$ have the $D0_{22}$ structure. Finally, for Y additions (Fig. 4(c)), the Bragg peaks of the $L1_2$ phase are shifted to lower angles with increasing Y content and the $D0_{19}$ phase appears at the highest Y content.

3.2. Solubility limits for the transition metals

XRD from powder samples and EDS analysis of individual phases from bulk samples can be used to estimate the solubility limit of ternary transition metal additions in Al_3Sc. The variation of lattice parameters of Al_3Sc with Y (Group IIIA), Ti (Group IVA) or V (Group VA) additions is shown in Fig. 5. In these figures, the lattice parameters of Al_3Ti, Al_3V or Al_3Y are experimental values reported by [1] and they are used in the lattice refinement of Al_3(X, Sc) as initial parameters. Furthermore, Fig. 6 shows the composition of the $L1_2$-Al_3Sc phase measured by EDS as a function of the ternary alloying element concentration.

Fig. 5(a) shows the lattice parameter change in $Al_3(Sc_{1-y}Ti_y)$ alloys. The lattice constant of the $L1_2$ phase decreases linearly with increasing Ti concentration. The composition of the $L1_2$ phase in Al_3Sc with Ti addition is shown in Fig. 6(a). The decreasing concentration of Sc in the $L1_2$ phase is compensated for by an increasing Ti concentration, while the Al concentration remains constant. From Fig. 5(a) and Fig. 6(a) and Table 1, we conclude that Ti replaces Sc in the $L1_2$ phase and the solubility limit of Ti in the $L1_2$ phase is somewhat below 12.5 at.% Ti ($y = 0.5$), corresponding to $Al_3(Sc_{0.5}Ti_{0.5})$. Addition of Ti in excess of this value results in the formation of the $D0_{22}$ phase, where the a-parameter decreases and c-parameter increases with increasing Ti concentration (Fig. 5(a)). Thus, the tetragonality of the $D0_{22}$ phase is increased by adding Ti as the c/a ratio increases from 2.21 to 2.23 from $Al_3(Sc_{0.5}Ti_{0.5})$ to $Al_3(Sc_{0.25}Ti_{0.75})$. For both Zr and Hf, the solubility limits are also somewhat below 12.5 at.% ($y = 0.5$), and the $D0_{23}$ phase is formed at a higher

Table 1
Phase composition (measured by EDS quantitative analysis) and lattice parameters (measured by XRD) for Al_3Sc and $Al_3(Sc_{1-y}X_y)$ with X = Ti, V, Y, Zr, Nb, Hf and Ta

Alloys	Structure	Chemical composition (at.%)			Volume fraction of $L1_2$	Lattice parameter (Å)	
		Al	Sc	X	f	a	c
Al_3Sc	$L1_2$	74.8 (1)	25.2 (1)	–	1.00	4.103 (1)	
		74.8[a]	25.2[a]	–			
$Al_3(Sc_{0.25}Ti_{0.25})$	$L1_1$	75.0 (1)	18.7 (2)	6.3 (3)	1.00	4.075 (2)	
$Al_3(Sc_{0.5}Ti_{0.5})$	$L1_2$	75.2 (6)	12.8(3)	12.0 (4)	<1.00[b]	4.036 (1)	
	$D0_{22}$	–	–		–	3.871 (3)	8.573 (4)
$Al_3(Sc_{0.25}Ti_{0.25})$	$D0_{22}$	74.7 (4)	4.7 (1)	20.6 (4)	0	3.849 (7)	8.583 (4)
Al_3Ti	$D0_{22}$	–	–	–	0	3.8537 (3)[c]	8.5839 (13)[c]
$Al_3(Sc_{0.9}V_{0.1})$	$L1_2$	75.0 (4)	23.3 (3)	1.7 (1)	0.96	4.098 (3)	
	$D0_{22}$	75.1 (6)	0.7 (1)	24.2 (7)	0.91 (6)[b]	3.781 (2)	8.340 (12)
$Al_3(Sc_{0.75}V_{0.25})$	$L1_2$	74.8 (3)	23.0 (2)	2.2 (2)	0.82	4.096 (5)	
	$D0_{22}$	74.6 (4)	0.7 (2)	24.7 (4)	0.81 (6)[b]	3.783 (2)	8.337 (7)
$Al_3(Sc_{0.5}V_{0.5})$	$L1_2$	74.8 (4)	22.5 (4)	2.7 (1)	0.56	4.096 (3)	
	$D0_{22}$	74.6 (4)	0.7 (1)	24.7 (3)	0.62 (2)[b]	3.782 (1)	8.338 (5)
Al_3V	$D0_{22}$	–	–	–	0	3.780[c]	8.321[c]
$Al_3(Sc_{0.9}Y_{0.1})$	$L1_2$	74.7 (2)	23.0 (1)	2.3 (3)	1.00	4.114 (1)	
$Al_3(Sc_{0.75}Y_{0.25})$	$L1_2$	74.7 (3)	19.9 (4)	5.4 (1)	1.00	4.138 (1)	
$Al_3(Sc_{0.5}Y_{0.5})$	$L1_2$	74.7 (6)	13.8 (6)	11.5 (2)	0.78	4.164 (1)	
	$D0_{19}$	75.2 (1)	8.7 (1)	16.1 (1)	0.86 (7)[b]	6.286 (9)	4.589 (8)
Al_3Y	$D0_{19}$	–	–	–	0	6.276 (2)[c]	4.582 (1)[c]
$Al_3(Sc_{0.75}Zr_{0.25})$	$L1_2$	74.8 (4)	19.9 (5)	5.4 (2)	1.00	4.095 (1)	
$Al_3(Sc_{0.5}Zr_{0.5})$	$L1_2$	74.7 (5)	13.1 (7)	12.2 (3)	0.96	4.092 (1)	
	$D0_{23}$	74.6 (4)	5.1 (4)	20.3 (1)	0.97 (3)[b]	3.999 (3)	17.262 (14)
$Al_3(Sc_{0.25}Zr_{0.75})$	$L1_2$	74.9 (6)	12.4 (7)	12.7 (4)	0.34	4.095 (1)	
	$D0_{23}$	74.9 (5)	3.23 (4)	21.8 (2)	0.34 (9)[b]	4.007 (1)	17.261 (5)
Al_3Zr	$D0_{23}$	–	–	–	0	4.009[c]	17.261[c]
$Al_3(Sc_{0.9}Nb_{0.1})$	$L1_2$	75.1 (3)	22.7 (1)	2.2 (1)	0.99	4.098 (8)	
	$D0_{22}$	75.2 (8)	1.9 (1)	22.9 (3)	0.91 (5)[b]	3.838 (3)	8.618 (9)
$Al_3(Sc_{0.75}Nb_{0.25})$	$L1_2$	75.0 (7)	23.4 (5)	1.6 (2)	0.79	4.098 (4)	
	$D0_{22}$	75.1 (4)	1.5 (4)	23.4 (4)	0.75 (4)	3.842 (1)	8.618 (3)
$Al_3(Sc_{0.5}Nb_{0.5})$	$L1_2$	75.1 (6)	23.2 (5)	1.6 (2)	0.52	4.095 (1)	
	$D0_{22}$	75.0 (2)	0.6 (1)	24.4 (2)	0.58 (1)[b]	3.840 (1)	8.617 (1)
Al_3Nb	$D0_{22}$	–	–	–	0	3.845[c]	8.601[c]
$Al_3(Sc_{0.9}Hf_{0.1})$	$L1_2$	75.2 (2)	22.3 (3)	2.5 (2)	1.00	4.095 (1)	
$Al_3(Sc_{0.75}Hf_{0.25})$	$L1_2$	75.3 (1)	19.0 (1)	5.7 (1)	1.00	4.091 (1)	
$Al_3(Sc_{0.5}Hf_{0.5})$	$L1_2$	75.4 (1)	12.0 (5)	12.6 (5)	0.99[b]	4.086 (1)	
	$D0_{23}$	–	–	–		3.999 (2)	17.138 (20)
Al_3Hf	$D0_{23}$	–	–	–	0	3.988[c]	17.157[c]
$Al_3(Sc_{0.9}Ta_{0.1})$	$L1_2$	74.5 (2)	23.8 (3)	1.7 (1)	0.96	4.096 (1)	
	$D0_{22}$	74.7 (5)	2.0 (1)	23.3 (4)	0.96 (2)[b]	3.845 (1)	8.578 (2)
$Al_3(Sc_{0.75}Ta_{0.25})$	$L1_2$	74.7 (5)	23.5 (7)	1.8 (2)	0.79	4.094 (1)	
	$D0_{22}$	74.6 (5)	2.1 (4)	23.3 (3)	0.83 (5)[b]	3.845 (1)	8.572 (3)
$Al_3(Sc_{0.5}Ta_{0.5})$	$L1_2$	74.7 (4)	23.7 (3)	1.6 (1)	0.50	4.094 (1)	
	$D0_{22}$	74.2 (1)	2.4 (1)	23.4 (3)	0.56 (1)[b]	3.844 (1)	8.572 (3)
Al_3Ta	$D0_{22}$	–	–	–	0	3.842[c]	8.553[c]

[a] Wet chemical analysis.
[b] Measured from microphotograph.
[c] Literature value [1].

concentration. From Table 1, it is clear that Sc in the $L1_2$ phase is replaced by Zr or Hf up to approximate compositions of $Al_3(Sc_{0.5}Zr_{0.5})$ or $Al_3(Sc_{0.5}Hf_{0.5})$. Nicholson et al. [14] reported that the Al_3Sc phase with a Zr addition has the $L1_2$ structure with a composition of $Al_{74.7}Sc_{9.4}Zr_{15.9}$. This solubility limit ($y = 0.63$) is larger than found in the present work ($y = 0.5$). On the other hand, Toropova et al. [15] estimate the maximum solubility of Zr in the $L1_2$ phase as $y = 0.4$, corresponding to $Al_3(Sc_{0.6}Zr_{0.4})$ and thus less than found in the present work. Their estimated solubility of Sc in the $D0_{23}$ phase is $y = 0.2$, in agreement with our range of values $y = 0.13$–0.20 (Table 1). Finally, a computational study based on first-principles total energy calculations predicts the thermodynamic stability of a cubic ternary alloy with composition $Al_3(Sc_{0.5}Zr_{0.5})$ [16].

Fig. 5(b) shows the lattice parameter change of $Al_3(Sc_{1-y}V_y)$. The lattice constant of the $L1_2$ phase decreases at first slightly with addition of V ($y = 0.1$), but remains almost unchanged for $y \geq 0.25$. As shown in Fig. 6(b), the decrease in Sc content in the $L1_2$ phase is nearly compensated for by an increase in V content for $y = 0.1$, with the Al content remaining constant. As shown in Fig. 5(b), the $D0_{22}$ phase appears already at the lowest V concentration ($y = 0.1$), and its a and c-parameters remain fairly constant for $y = 0.1$–1. This

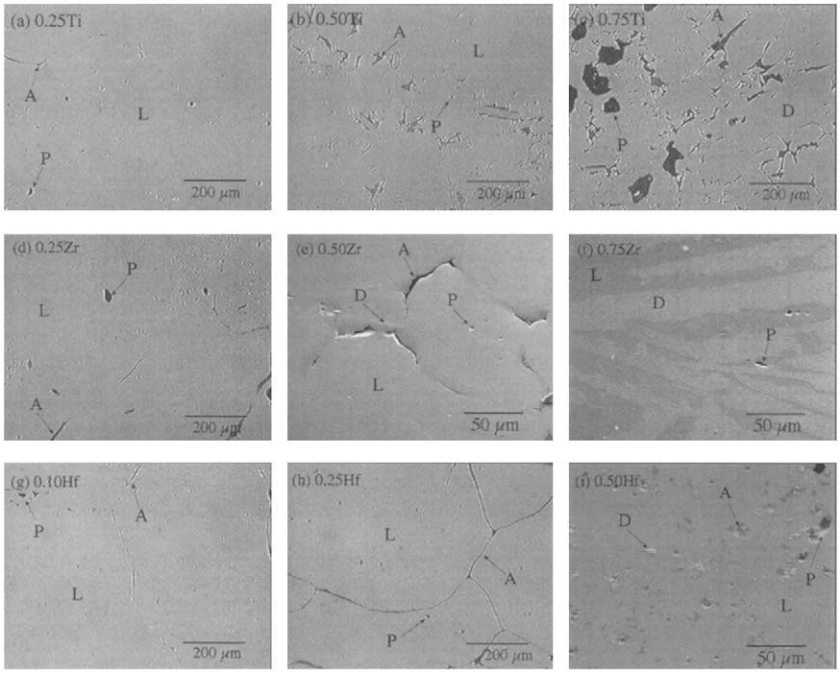

Fig. 2. Typical microstructures of homogenized $Al_3(Sc_{1-y}X_y)$ where X is Ti, Zr, and Hf for $y = 0.10$, 0.25, 0.50 and 0.75. (A: Al phase, L: $L1_2$ phase, D: $D0_{22}$ phase (Ti), $D0_{23}$ phase (Zr, Hf) and P: porosity).

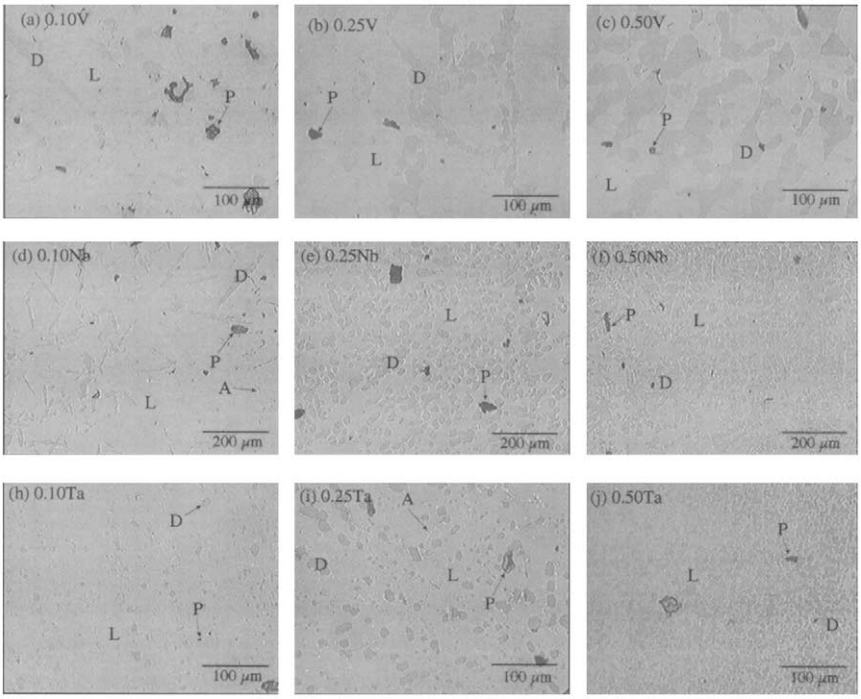

Fig. 3. Typical microstructures of homogenized $Al_3(Sc_{1-y}X_y)$ with X = V, Nb and Ta for $y = 0.10$, 0.25 and 0.50. (A: Al phase, L: $L1_2$ phase, D: $D0_{22}$ phase and P: porosity).

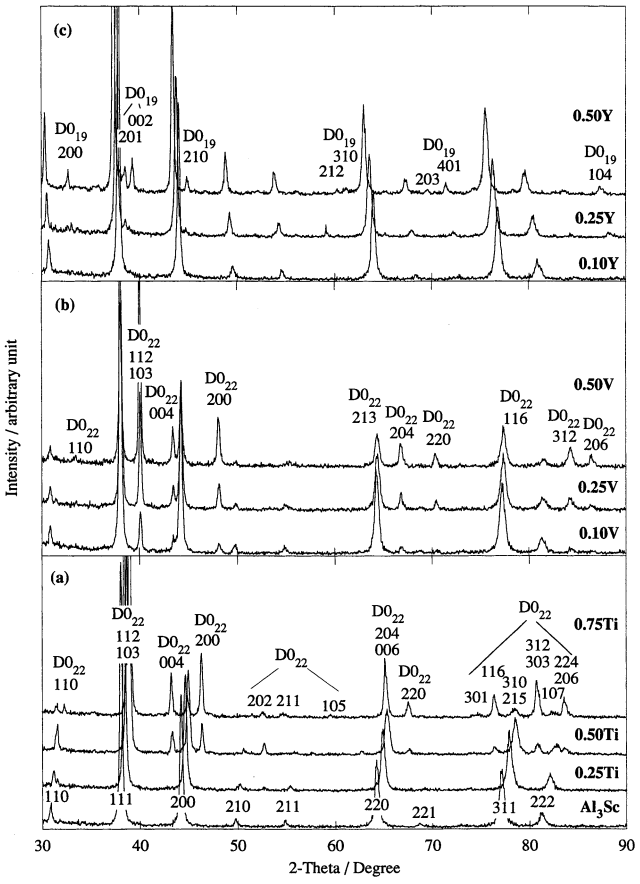

Fig. 4. Typical X-ray diffraction patterns of $Al_3(Sc_{1-y}X_y)$ with X = (a) Ti, (b) V and (c) Y additions for $y = 0.10$, 0.25, 0.50 and 0.75.

suggests that both the $L1_2$ and $D0_{22}$ phases have a low solubility limit for ternary elements; 2.7 at.% V in the $L1_2$ phase $Al_3(Sc_{0.89}V_{0.11})$, and 0.7 at.% Sc in the $D0_{22}$ phase $Al_3(V_{0.97}Sc_{0.03})$ (Table 1). The lattice parameter change for $D0_{22}$ phase Al_3(Sc, V) was similar to those for the $D0_{22}$ phases Al_3(Sc, Nb) and Al_3(Sc, Ta). These two phases also have low solubility limits for Sc: about 1.8 at.% Sc in $Al_3(Nb_{0.95}Sc_{0.05})$ and 2.2 at.% Sc in $Al_3(Ta_{0.91}Sc_{0.09})$. Conversely, the $L1_2$ phase has low solubility for Nb (about 2.2 at.% Nb, $y = 0.09$) and for Ta (about 1.8 at.% Ta, $y = 0.07$). For the Nb addition, these results are in reasonable agreement with the compositions $Al_{75.7}Sc_{23.5}Nb_{0.8}$ ($L1_2$) and $Al_{75.7}Nb_{23.0}Sc_{1.3}$ ($D0_{22}$) reported by Nicholson et al. [14].

In the case of Y additions (Fig. 5(c)), the lattice constant of the $L1_2$ phase increases with increasing Y concentration, in contrast to the six other metals we investigated. For $y = 0.5$, the $D0_{19}$ phase is observed. As shown in Fig. 6(c), the decreasing level of Sc in $L1_2$ phase is compensated linearly by an increasing Y level, while the Al concentration remains constant. This suggests that the solubility limit of Y in the $L1_2$ phase is somewhat below 12.5 at.% ($y = 0.5$) and that the $L1_2$ phase transforms to the $D0_{19}$ phase with increasing Y concentration. This phase has a relatively high solubility for Sc (8.7 at.% Sc), corresponding to $Al_3(Y_{0.74}Sc_{0.26})$.

Table 1 summarizes the lattice parameters and the EDS quantitative analyses of binary Al_3Sc and the ternary alloys. From the experimentally measured phase composition, the volume fraction of the $L1_2$ phase was calculated by mass conservation. Reasonable

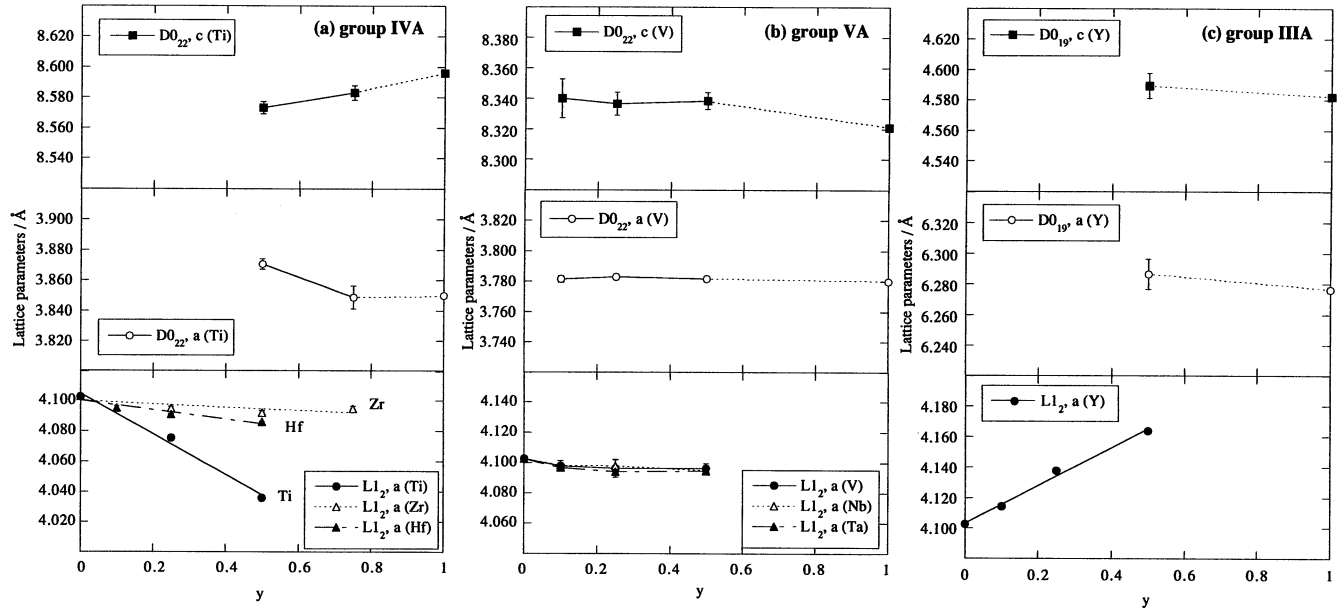

Fig. 5. Lattice parameters in $Al_3(Sc_{1-y}X_y)$ as a function of the total concentration y for (a) X = Ti, Zr, Hf, (b) X = V, Nb, Ta and (c) X = Y additions.

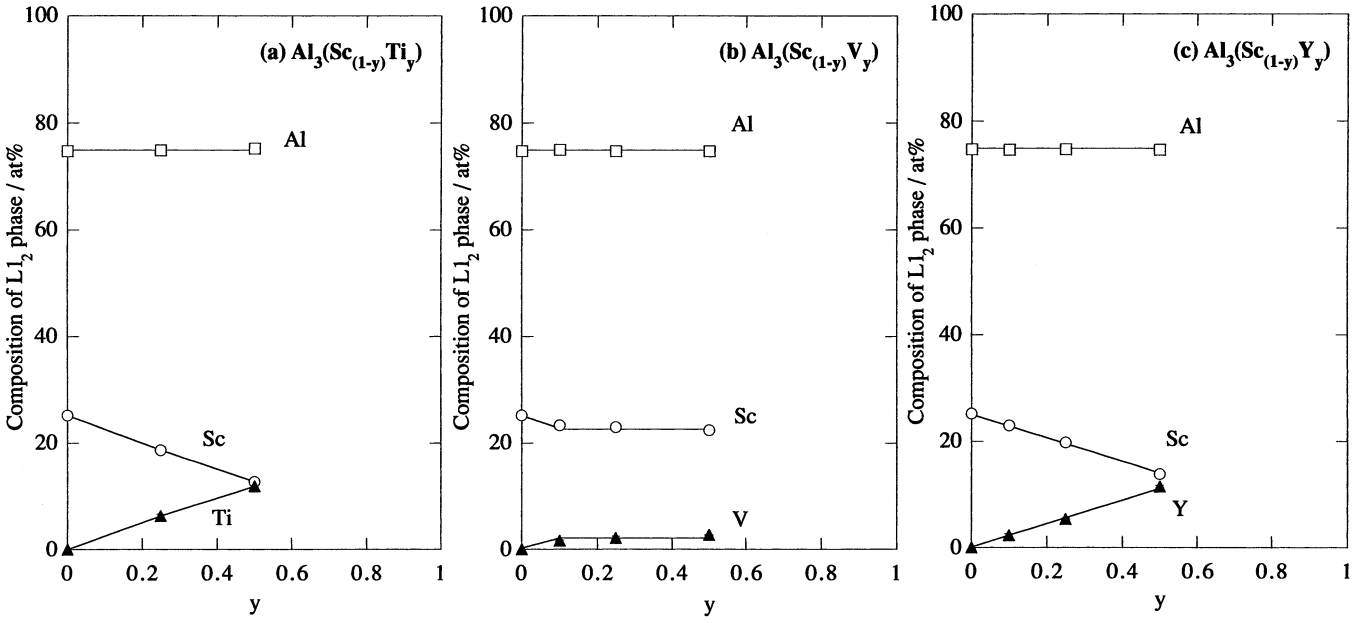

Fig. 6. Composition of $L1_2$ phase in $Al_3(Sc_{1-y}X_y)$ as a function of total concentration y for (a) X = Ti, (b) X = V and (c) X = Y.

agreement is found with values found independently from image analysis of optical micrographs.

In summary, metals from Groups IIIA (Y), IVA (Ti, Zr, Hf) and VA (V, Nb, Ta) can be incorporated substitutionally in the Sc sublattice of Al_3Sc as shown in Figs. 4–6. Binary trialuminides of these metals have long period structures ($D0_{19}$, $D0_{22}$ and or $D0_{23}$ structures), which are related closely to the cubic $L1_2$ structure. It has been reported that Ti, Y, Zr and Hf trialuminides can form a metastable phase with the $L1_2$ structure [17,18]. Our results indicate that the solid solubility in the $L1_2$ phase varied systematically with the location of the ternary alloying element in the periodic table. For example, Y (Group IIIA) and Ti, Zr and Hf (Group IVA) are located near Sc (Group IIIA) and have a larger solid solubility in Al_3Sc, than V, Nb or Ta (Group VA).

Considering these observations, it appears that ternary alloying elements X, which can substitute substantially for Sc in Al_3Sc, need to form binary trialuminides Al_3X with the $L1_2$ structure and/or be located near Sc in the periodic table. The trialuminides of the rare-earth elements Er, Yb and Lu crystallize in the $L1_2$ structure, while Al_3La has the closely related $D0_{19}$ structure [1]. These alloying elements are thus good candidates to replace substitutionally Sc in $L1_2$ ternary $Al_3(Sc, X)$ trialuminides. Conversely, it is known that $D0_{22}$-Al_3Ti where Al is substituted partially for by Cr, Mn, Fe, Co or Ni [2–4] and $D0_{23}$-Al_3Zr, where Al is replaced by Cr, Fe, Ni or Cu [19], can be transformed to the cubic $L1_2$ structure. These alloying elements are then also good candidates to replace substitutionally Al in $(Al, X)_3Sc$ with the $L1_2$ structure.

3.3. Lattice parameter as a function of ternary transition metals

Fig. 7 shows the relationship between the concentration of ternary transition metal in the $L1_2$ phase (measured by EDS) and the lattice parameter of the $L1_2$ phase (measured by XRD). This figure shows that there is a linear relationship between lattice parameter and concentration for Ti, Y, Zr or Hf, which have large solubility limits of up to 12.5 at.% ($y = 0.5$). For the Group IVA metals (Ti, Zr and Hf), the lattice parame-

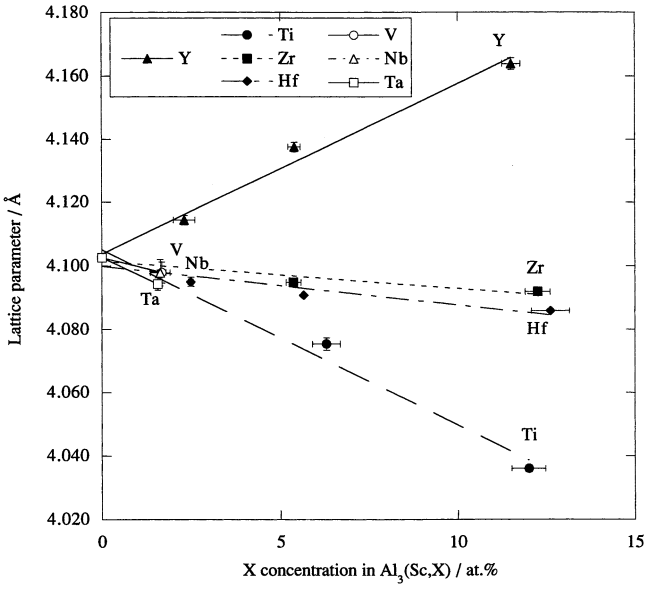

Fig. 7. Lattice parameter of the $L1_2$ phase in $Al_3(Sc, X)$ as a function of ternary transition-metal additions.

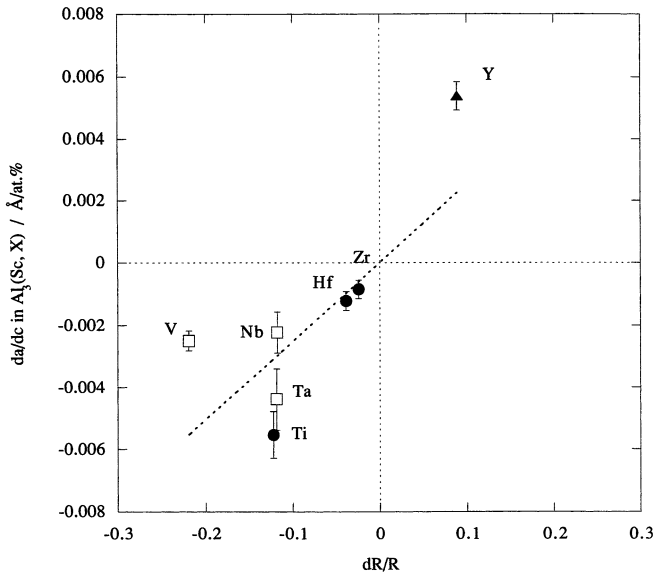

Fig. 8. Relationship between the atomic radius mismatch, dR/R, and the composition dependence of $L1_2$ lattice parameter, da/dc.

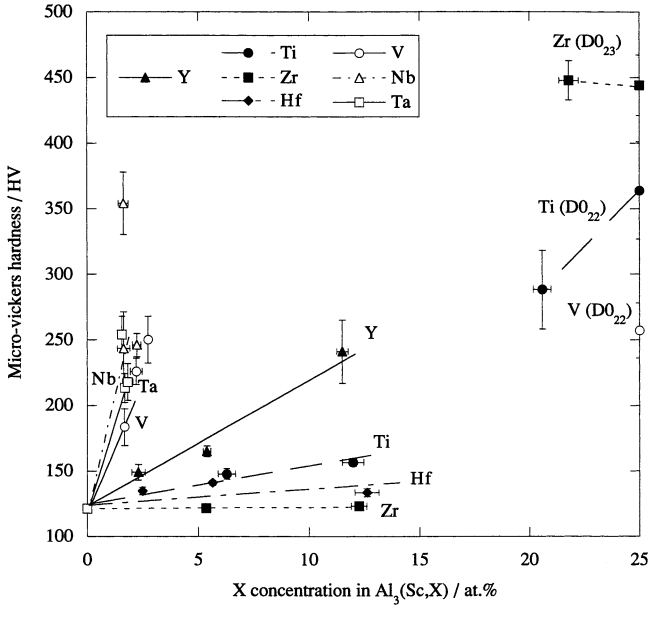

Fig. 9. Vickers microhardness of $L1_2$ phases in $Al_3(Sc, X)$, except where noted, as a function of ternary transition-metal concentration.

ter decreases with increasing concentration. The lattice variation with Zr or Hf additions is much smaller than with Ti additions. Conversely, additions of Y (Group IIIA) increase the lattice parameter of Al_3Sc and the magnitude of the change is about as large as for Ti. Similar to the Group IVA metals, the Group VA metals (V, Nb and Ta) induce a decrease of the $L1_2$ lattice parameter. Due to their limited solubility limit (about 2.5 at.%, $y = 0.1$), it is difficult to quantify the effect, but the concentration dependence seems to be similar for Ta and Ti, and similar for V (or Nb) and Zr (or Hf).

From the linear relationship between concentration, c, and lattice parameter, a, of the solid-solution $L1_2$ phase (Fig. 7), a best-fit slope, da/dc, is determined. Fig. 8 shows that this slope, i.e. the composition dependence of $L1_2$ lattice parameter, correlates reasonably well with the relative atomic radius mismatch, $dR/R = (R_{Sc} - R_X)/R_X$, where R is the metallic hard-sphere radius from [20] (no significant difference was found in the correlation when ionic Pauling's radii were used). A similar correlation was found by Yamamoto et al. [21] for the $L1_2$ quaternary phase $\{(AlMn)_3Ti\}_{(1-n)}X_n$, where X is Zr, V, Ag or Ga. This correlation can be understood in terms of the size mismatch associated with the replacement of solvent atoms with solute atoms causing a distortion of the lattice. The resulting strain field may allow solute atoms to interact strongly with dislocations and to affect their motion, thus impacting on the strength of the solid solution, as discussed in the following section.

3.4. Microhardness as a function of ternary transition metals

The Vickers microhardness of binary Al_3Sc was found to be 121 ± 3 HV (HV = 9.80 MPa). This value is very close to the value (111 ± 8 HV) reported by Nic et al. [3] but lower than the value (140 HV) reported by Schneibel et al. [22] for drop-cast Al_3Sc. We note that Al_3Sc is significantly less hard than $D0_{22}$-Al_3Ti (364 ± 37 HV), $D0_{22}$-Al_3V (257 ± 21 HV) or $D0_{23}$-Al_3Zr (444 ± 23 HV) as well as ternary-element modified Ll_2-Al_3Ti (from 151 HV for Cr to 220 HV for Ni) [3].

Fig. 9 shows the microhardness of alloyed Al_3Sc as a function of the concentration of transition metals in the ternary $L1_2$ phase (as obtained by EDS). While all elements harden the binary Al_3Sc compound, the effect is dependent upon the position in the periodic table. Group IVA metals have the lowest hardening effect, which is, within experimental error, null for Zr and modest for Hf or Ti (but somewhat larger for Ti). Yttrium (Group IIIA) has a significantly larger effect as the hardness is doubled from Al_3Sc to $Al_3(Sc_{0.50}Y_{0.50})$. For the four metals with a large solubility in the $L1_2$ phase, Fig. 9 shows that the hardness increases linearly with ternary concentration. The largest hardening effect is associated with the Group VA metals (V, Nb or Ta), which, however, have limited solid solubility in the $L1_2$ phase. For V additions, the hardest $L1_2$ composition $Al_3(Sc_{0.89}V_{0.11})$ is as hard as the $D0_{22}$ binary trialuminide Al_3V and more than twice as hard as binary Al_3Sc. By contrast, the binary $D0_{22}$-Al_3Ti or $D0_{23}$-Al_3Zr have much higher microhardness than the alloyed $L1_2$-Al_3Sc where half the Sc has been replaced by Ti or Zr.

The relative effectiveness of ternary additions on solid-solution hardening is quantified by the slope of the best-fit straight line, dHV/dc, in Fig. 9. For the low-solubility metals V, Nb or Ta, only the lowest hardness point was considered, because it is possible that a small volume fraction of a finely dispersed hard second-phase, not visible in the optical micrographs, could increase hardness by dispersion strengthening, especially for the high hardness data point for Nb.

In considering the degree of the solid solution hardening of the ternary alloys, the atomic size effect would be the first criterion to take into account. However, the hardness effects are not related in a simple manner to atomic size effect as in binary alloys since the different substitution behavior of different elements must be considered.

Fig. 10 shows the correlation between the concentration dependence of microhardness, dHV/dc, and lattice strain, da/dc, in alloyed Al_3Sc. For Group IVA metals (Ti, Zr or Hf), a best-fit straight line is drawn and shows a good correlation, indicative of a first-order elastic interaction between dislocations and solute atoms. For the Group VA metals (V, Nb or Ta), the correlation is poor, possibly because of the significant experimental errors on both da/dc (due to low solubility) and dHV/dc (due to possible dispersion hardening). However, it is clear that the lattice strain is not the only parameter controlling hardness, since the Groups IIIA, IVA and VA are clearly separated from each other in Fig. 10. Valence effects must be operative as well, as also suggested for alloyed $L1_2$-Ni_3Al. For Ni_3Al containing ternary transition-metal additions, Mishima et al. [23] found a correlation between the rate of solid-solution hardening, dσ/dc, and the lattice parameter change, da/dc, for elements of the same period. Huang et al. [24] found a good correlation for Ti, V, Cr, Fe, as well B, C, Si, the magnitude of which was in reasonable agreement with the Mott–Nabarro model of solid-solution strengthening. Similarly, Guard et al [25]. found a roughly linear relation between the rate of hardness change and lattice strain for a variety of ternary alloying additions, except for Cr and Mo.

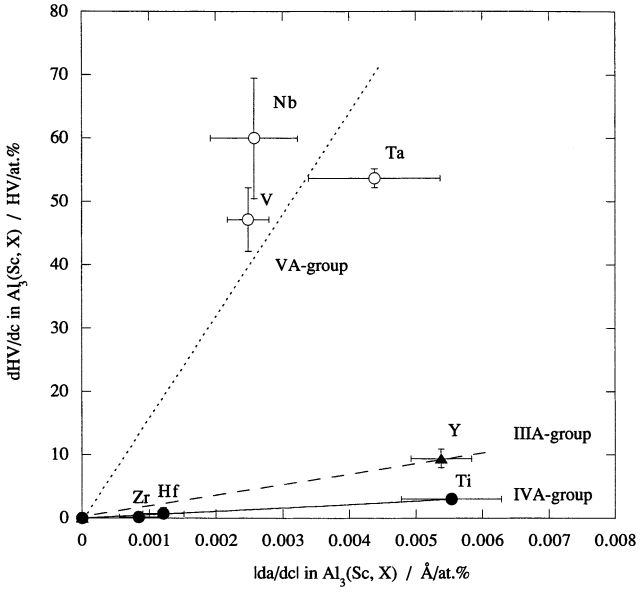

Fig. 10. Correlation between composition dependence of microhardness and concentration dependence of lattice strain in $L1_2$-Al_3(Sc, X).

In an earlier paper, we investigated the compressive creep behavior for $Al_3(Sc_{0.74}X_{0.26})$, where X is Ti, Y, Zr or Hf [9]. At 873 K, a decrease in creep rates of one order of magnitude was found for Zr and Hf, and two orders of magnitude for Ti and Y. These trends are in reasonably good agreement with the room temperature hardness values (Fig. 9). The exact mechanism responsible for solid-solution strengthening at ambient and elevated temperatures must await precise observations of dislocations in indented or compressively-deformed specimens, as many factors may be operating, e.g. interaction of solute atoms with vacancies and dislocation jogs, segregation on stacking faults and increase of the Peierls stress.

4. Conclusions

The microstructure of the ternary trialuminide $Al_3(Sc_{1-y}X_y)$, where X is a transition metal from Groups IIIA (Y), IVA (Ti, Zr, Hf) or VA(V, Nb, Ta), was investigated as a function of alloying element concentration in the range $0 \le y \le 0.75$. The following conclusions are drawn.

Alloys with Groups IIIA (Y) or IVA (Ti, Zr, Hf) additions exhibit an as-cast microstructure consisting of a single majority $L1_2$ phase with a low volume fraction of an Al-phase at grain boundaries. As a result of a subsequent homogenization treatment, Kirkendall porosity developed and the alloys are single-phase up to $y = 0.5$. At the highest alloying level ($y = 0.75$), new ternary aluminides Al_3(X, Sc) are formed with the $D0_{22}$ (Ti), $D0_{19}$ (Y) or $D0_{23}$ (Zr and Hf) structures. Alloys with Group VA additions (V, Nb, Ta) show both the $L1_2$ phase and a dendritic second phase with the $D0_{22}$ structure for the lowest concentration studied ($y = 0.1$).

The solubility limit of Groups IIIA and IVA metals in the $L1_2$ phase $Al_3(Sc_{1-y}X_y)$ is high, somewhat below 12.5 at.% ($y = 0.5$). The solubility of Group VA metals V, Nb and Ta is much lower and varies from about 1.8 at.% ($y = 0.07$) for Ta to about 2.7 at.% ($y = 0.11$) for V.

The solubility of Sc in the non-$L1_2$ phases $Al_3(X_{1-y}Sc_y)$ is substantial in the Groups IIIA and IVA trialuminides (from 3.2 at.% for Al_3(Zr, Sc) to 8.7 at.% for Al_3(Y, Sc)), but low in the Group VA trialuminides (between 0.6 and 2.2 at.%).

The lattice parameter of the $L1_2$ phase $Al_3(Sc_{1-y}X_y)$ decreases linearly with Group IVA or VA element concentration, but increases linearly with Y (Group IIIA) concentration. The concentration dependence of the lattice parameter correlates well with the atomic size mismatch between Sc and the alloying element.

The Vickers microhardness of the $L1_2$ phase $Al_3(Sc_{1-y}X_y)$ increases linearly with increasing ternary concentration. At a given concentration, the Group IVA metals have the lowest hardening effect, and the Group VA metals have the highest effect, with Y (Group IIIA) being intermediate. The concentration dependencies of hardness and lattice parameter (i.e. lattice strain) are correlated for the Group IVA metal.

Acknowledgements

This research was supported by the Division of Materials Science, United States Department of Energy under contract DE-FG02-98ER45721. Y. Harada greatly appreciates the support of the Japan Society for the Promotion of Science for Young Scientists in the form of a Research Fellowship. Useful discussions with Professor M. Asta and Professor D.N. Seidman (Northwestern University) are also gratefully acknowledged.

References

[1] P. Villars, L.D. Calvert, Pearson's Handbook of Crystallographic Data for Intermetallic Phases, ASM, Metal Park, OH, 1985.
[2] E.P. George, D.P. Pope, C.L. Fu, J.H. Schneibel, ISIJ Int. 31 (1991) 1063.
[3] J.P. Nic, S. Zhang, D.E. Mikkola, in: L.A. Johnson, D.P. Pope, J.O. Stiegler (Eds.), High Temperature Ordered Intermetallic Alloys IV, MRS, Pittsburgh, PA, 1990, p. 697.
[4] Y. Nakayama, H. Mabuchi, Intermetallics 1 (1993) 41.
[5] J.H. Schneibel, J.A. Horton, W.D. Porter, Mater. Sci. Eng. A152 (1992) 126.
[6] S. Zhang, J.P. Nic, D.E. Mikkola, Scripta Metall. Mater. 24 (1990) 57.
[7] K. Fukunaga, T. Shouji, Y. Miura, Mater. Sci. Eng. A239–240 (1997) 202.
[8] J.H. Schneibel, P.M. Hazzledine, J. Mater. Res. 7 (1992) 868.
[9] Y. Harada, D.C. Dunand, Acta Mater. 48 (2000) 3477.
[10] C.B. Fuller, D.N. Seidman, D.C. Dunand, Scr. Mater. 40 (1999) 691.
[11] L.S. Toropova, D.G. Eskin, M.L. Kharakterova, T.V. Dobatkina, Advanced Aluminum Alloys Containing Scandium, Gordon and Breach Science Publisher, Amsterdam, 1998.
[12] T.B. Massalski, J.L. Murray, L.H. Bennett, H. Baker, Binary Alloy Phase Diagrams, American Society for Metals, Metals Park, OH, 1986, p. 161.
[13] K. Kita, G. Itoh, M. Kanno, in: J.A. Horton, I. Baker, S. Hanada, R.D. Noebe, D.S. Schwartz (Eds.), High Temperature Ordered Intermetallic Alloys VI, MRS, Pittsburgh, PA, 1995, p. 1241.
[14] D.M. Nicholson, J.H. Schneibel, W.A. Shelton, in: G.M. Stocks, D.P. Pope, A.F. Giamei (Eds.), Alloy Phase Stability and Design Symposium, MRS, Pittsburgh, PA, 1991, p. 229.
[15] L.S. Toropova, A.N. Kamardinkin, V.V. Kindzhibalo, A.T. Tyvanchuk, Phys. Met. Metall. 70 (1990) 106.
[16] J.-H. Xu, A.J. Freeman, Phys. Rev. B41 (1990) 12553.
[17] S. Srinivasan, P.B. Desch, R.B. Schwarz, Scr. Metall. Mater. 25 (1991) 2513.
[18] J.C. Foley, J.H. Perepezko, D.J. Skinner, Mater. Sci. Eng. A179/A180 (1994) 205.
[19] J.H. Schneibel, W.D. Porter, in: C.T. Liu, A.I. Taub, N.S. Stoloff, C.C. Koch (Eds.), High Temperature Ordered Intermetallic Alloys III, MRS, Pittsburgh, PA, 1988, p. 335.
[20] E.T. Teatum, K.A. Gshneidner, J.T. Waber, Report of Los Alamos Scientific Laboratory of the University of California, LA-2345, Department of Commerce, Washington, DC, 1968.
[21] Y. Yamamoto, K. Hashimoto, T. Kimura, H. Moriya, M. Nobuki, N. Kohno, J. Jpn. Inst. Metals 62 (1998) 844.
[22] J.H. Schneibel, E.P. George, Scr. Metall. Mater. 24 (1990) 1069.
[23] Y. Mishima, S. Ochiai, M. Yodogawa, T. Suzuki, Trans. JIM 27 (1986) 41.
[24] S.C. Huang, C.L. Briant, K.-M. Chang, A.I. Taub, E.L. Hall, J. Mater. Res. 1 (1986) 60.
[25] R.W. Guard, J.H. Westbrook, Trans. Metall. Soc. AIME 215 (1959) 807.